The Vorticity Budget of a Composite African Tropical Wave Disturbance

LLOYD J. SHAPIRO

National Hurricane and Experimental Meteorology Laboratory, NOAA, Coral Gables, Fla. 33124

(Manuscript received 19 September 1977, in final form 17 January 1978)

ABSTRACT

Composite fields of large-scale variables derived from synoptic-scale wave disturbances observed during Phase III of the GARP Atlantic Tropical Experiment over Africa and the eastern Atlantic are used to determine the vorticity budget of the composite African wave. The velocity, vorticity and divergence fields used are "combined region" composites of the wave disturbances derived by Norquist *et al.* (1977).

The vorticity budget is made for all eight categories (phases) of the wave at the reference latitude (~11°N) as well as the latitudes 4° to the north and south of the reference latitude. The large-scale fields are decomposed into a zonal mean and deviations from the zonal mean to separate contributions from the wave and the basic flow in which it is embedded. Cumulus mass fluxes (derived by R. Johnson) are determined from a thermodynamic budget and a spectral cloud model. The average vorticity in the clouds is determined from a simple one-dimensional single-cloud model using the given cumulus mass fluxes. Since cumulus mass fluxes and vorticities are determined independently of the large-scale vorticity budget, the parameterized vorticity source due to cumulus is not forced to equal the apparent vorticity source derived from the large-scale balance.

It is found that the large-scale vorticity balance for the wave is linear, with the nonlinear horizontal advective terms approximately cancelling due to the presence of a quasi-nondivergent, single-propagating wave component. The linear waves are approximately advected by the horizontal wind at all levels above 850 mb, even to the south of the easterly jet where the mean zonal wind is small. The curvature term contributes significantly to the balance. The parameterized form of the vertical advection of vorticity due to cumulus accounts well for most features of the apparent vorticity source obtained from the large-scale budget when the vertical cumulus mass flux is specified only for deep clouds. The large apparent source ahead of the trough in the middle troposphere at 11°N is reflected in the parameterized form. Cumulus-scale twisting effects are not needed to explain the major part of the large-scale apparent vorticity source, except possibly near the tropopause.

1. Introduction

Observations made during the GARP Atlantic Tropical Experiment (GATE) have provided a data base that can be used to obtain an increased understanding of the interaction between synoptic-scale tropical disturbances and the cumulus scale as well as the environment in which the disturbances are embedded. The parameterization of the effect of cumulus-associated eddies on the synoptic-scale momentum or vorticity balance is a question of fundamental importance to numerical and theoretical modeling (e.g., Stevens *et al.*, 1977). An analysis of the interaction between the synoptic-scale systems and the basic-state "general circulation" is necessary for the complete understanding of changes in the structure of the disturbances, as well as the possible development of some of the disturbances into tropical storms. Burpee (1975) has presented synoptic-scale wave composites covering the entire GATE experiment. The structure and energetics of synoptic-scale tropical wave disturbances that were observed during Phase III of GATE (23 August–19 September 1974) over Africa and the eastern Atlantic have been analyzed by Reed *et al.* (1977), hereafter referred to as RNR, and Norquist *et al.* (1977). The data set used in their analyses described an "average" wave composited from eight disturbances that propagated westward across western Africa and the adjacent oceanic region. The GATE Quick Look Data Set was used as the data base. Unlike previous studies of a composite Pacific wave disturbance (Reed and Recker, 1971; Reed and Johnson, 1974), the description of the African wave is unique in its inclusion of the meridional as well as zonal and vertical structure for all velocity fields.

The present study analyzes the vorticity budget of the composite African wave disturbance using velocity, vorticity and divergence fields derived by Norquist *et al.* (1977) as "combined region" composites. The fields were provided by the authors. These combined region fields, described completely in Section 3 of Norquist *et al.* (1977), are composites for the land and ocean regions taken together above 700 mb (as also used in RNR), and an average between the land and ocean regions composited separately below 700 mb.

The vorticity budget is computed for all phases ("categories") of the composite wave at the reference latitude (~11.5°N) as well as latitudes 4° to the north and south of the reference latitude. In the following these latitudes will be referred to as 11, 15 and 7°N, respectively, even though this is only an approximation (cf. RNR's Section 2).

The purpose of the present analysis is to determine the large-scale vorticity budget of the composite African wave, the degree to which very simply parameterized cumulus-associated eddies can account for the imbalance that exists on the large scale, as well as the relation between the wave and the basic flow in which it moves.

Vorticity budgets of synoptic-scale systems have previously been made by Yanai and Nitta (1967) and Hawkins (1972), among others. Reed and Johnson (1974, hereafter referred to as RJ) determined the vorticity budget of a composite synoptic-scale wave in the western Pacific, including a simple parameterized form of cumulus vorticity transports. The present analysis differs from their study in several respects:

1) The large-scale fields are decomposed into a zonal mean and deviations from the zonal mean to separate contributions from the wave and the basic flow in which it is embedded. The importance of individual terms, in particular nonlinear terms, in the vorticity balance, as well as total (wave plus mean) terms are evaluated.

2) Horizontal gradients of all fields in the meridional as well as zonal direction are included. In particular the complete advective term is evaluated.

3) Cumulus mass fluxes (derived by R. Johnson) are determined from a spectral cloud model and a thermodynamic budget. The average vorticity in the clouds is determined from a one-dimensional single-cloud model using the given cumulus mass fluxes.

4) Since cumulus mass fluxes and vorticities are determined independently of the large-scale vorticity budget, the parameterized vorticity source due to cumulus is not forced to equal the apparent vorticity source derived from the large-scale balance. The parameterized source term is compared with the apparent source term to determine how well the parameterized form approximates the apparent source.

2. Large-scale budget

The vorticity equation in pressure coordinates is

$$\eta_t+\nabla\cdot(\eta\mathbf{V})+\omega\eta_p+\mathbf{k}\cdot\nabla\omega\times\mathbf{V}_p=0, \qquad (1)$$

where $\eta=f+\zeta$ is the absolute vorticity, the sum of the Coriolis parameter f and the relative vorticity ζ; $\mathbf{V}=(u,v)$ is the horizontal velocity, p the pressure, ω the vertical velocity in pressure coordinates, t time, ∇ the horizontal gradient and $\mathbf{k}$ the unit vertical vector. Following Yanai *et al.* (1973), RJ and many others, Eq. (1) is averaged over an area A that is large enough to contain many convective elements but small enough to be considered local on the synoptic scale. Denoting the area average by an overbar A, deviations from the average by a double prime and using the continuity equation, Eq. (1) becomes

$$Z\equiv\bar{\zeta}^A_t+\bar{\mathbf{V}}^A\cdot\nabla\bar{\eta}^A+\bar{\omega}^A\bar{\zeta}^A_p+\bar{\eta}^A\bar{\delta}^A+\mathbf{k}\cdot\nabla\bar{\omega}^A\times\bar{\mathbf{V}}^A_p$$
$$=-\overline{\nabla\cdot(\mathbf{V}''\zeta'')}^A-\overline{\omega''\zeta''_p}^A-\mathbf{k}\cdot\overline{\nabla\omega''\times\mathbf{V}''_p}^A. \qquad (2)$$

The divergence $\bar{\delta}^A\equiv\nabla\cdot\bar{\mathbf{V}}^A$. The nonstandard notation for the averaging is used to avoid later confusion. In the following, large-scale averaged variables will be denoted without an overbar (e.g., $\zeta\equiv\bar{\zeta}^A$) for simplicity. Z, the residual of the large-scale vorticity budget, represents the "apparent vorticity source" (RJ) for the large scale by subsynotic scale eddies. The subsynoptic processes that balance the large-scale residual above the boundary layer are considered to be associated with cumulus-scale motions. The parameterization of the cumulus-scale eddy correlation terms in (2) in terms of large-scale variables will be investigated in Section 3. In this section only the large-scale balances (or imbalances) will be considered. The large-scale terms in (2) represent, respectively, the local change of vorticity, the horizontal advection of (absolute) vorticity, vertical advection, vorticity divergence (vortex tube stretching) and twisting effects.

The terms in the large-scale vorticity budget at 11°N are presented in Fig. 1. The large-scale twisting terms are found to be very small and are not presented. The categories refer to approximate phases of the wave. Category 4 is at the 700 mb vorticity maximum and is approximately at the wave trough; category 8 is at the ridge. Zonal gradients are based on the observed average zonal wavelength of 2500 km, corresponding to about 300 km between wave categories. Local time changes are based on an average period of 3.5 days. The zonal phase speed (assumed constant) is about -8 m s^{-1}. The amplitude of the local time change (Fig. 1a) is 27×10^{-11} s^{-2}. This value is consistent with the vorticity amplitude of about 1.5×10^{-5} s^{-1} and the period of 3.5 days, but is very much larger than the local vorticity tendencies found by RJ and Ruprecht and Gray (1976). Their analyses concentrated on the trough or ridge (cloudy or clear) regions where the vorticity tends to be a maximum or minimum. The extrema of ζ_t occur near categories 2 and 6, which are intermediate between the trough and the ridge. Nevertheless, Fig. 1b indicates that ζ_t is balanced quite well by horizontal advection at all phases of the wave, except below 800 mb and above 250 mb. The maximum value of $\zeta_t+\mathbf{V}\cdot\nabla\eta$ in the middle troposphere is 7×10^{-11} s^{-2}, less than 30% of ζ_t. It will be seen below that the balance at 7°N is not as complete. The vertical advective term, shown in Fig. 1c, has a maximum value of about 8×10^{-11} s^{-2} near 300 and 800 mb. The sum of the large-scale terms is dominated by vorticity diver-

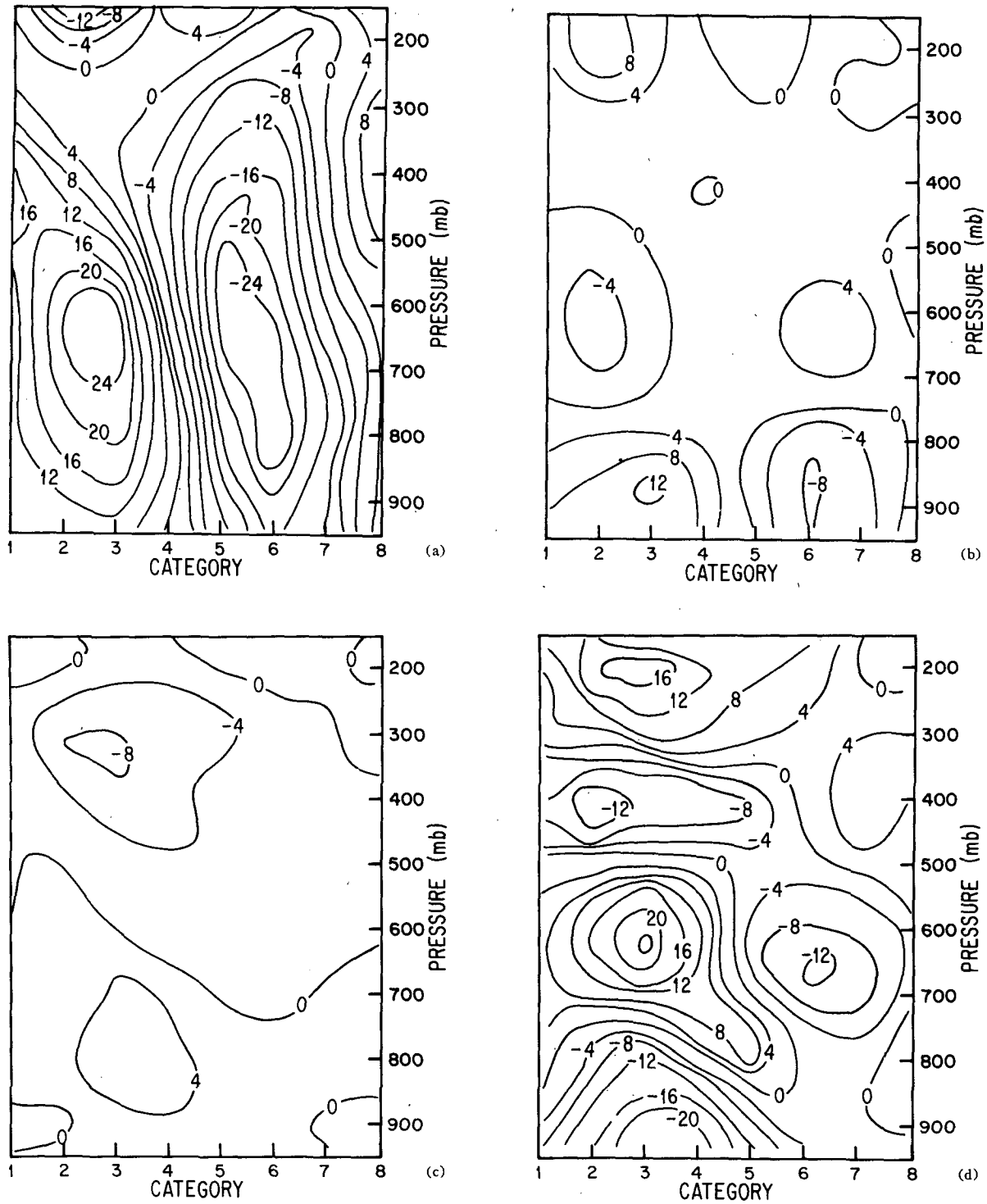

FIG. 1. (a) ζ_t at reference latitude, 11°N (10^{-11} s^{-2}), (b) $\zeta_t + \mathbf{V}\cdot\nabla\eta$ at 11°N (10^{-11} s^{-2}), (c) $\omega\zeta_p$ at 11°N (10^{-11} s^{-2}), (d) $\eta\delta$ at 11°N (10^{-11} s^{-2}).

gence, shown in Fig. 1d, where the pattern of $\eta\delta$ follows that of the divergence as described by RNR. The dominance of $\eta\delta$ is consistent with RJ's finding for a composite Pacific wave disturbance. Large values of $\eta\delta$ have been found in all vorticity budget studies of disturbances with significant convective activity (e.g., RJ; Hawkins, 1972). The residual Z, the apparent vorticity source, is shown in Fig. 2 for 11°N and is very similar to $\eta\delta$ in Fig. 1d. A negative residual in the lower troposphere and a positive residual in the upper, seen in Fig. 2, were also found by RJ. The large positive value (24×10^{-11} s^{-2}) ahead of the trough in the middle

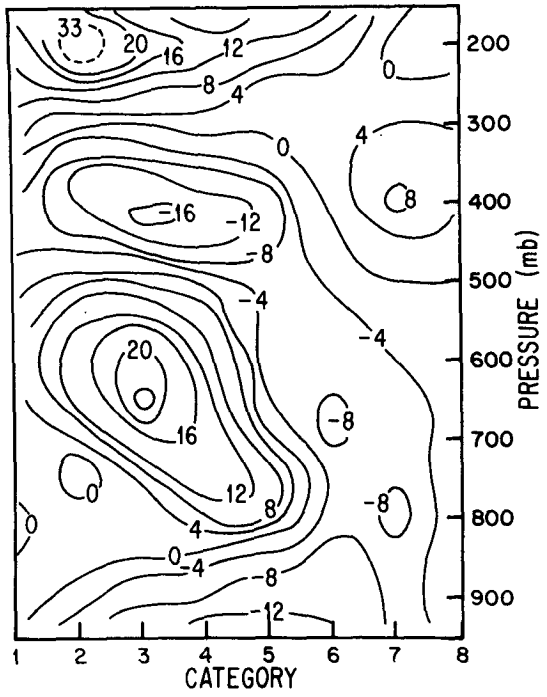

FIG. 2. Apparent vorticity source Z at 11°N (10^{-11} s^{-2}).

troposphere corresponds to the divergence maximum found by RNR. It has no precedent in previous vorticity budget studies and indicates the complexity of Z that must be accounted for by the cumulus scale. In Fig. 3 the apparent vorticity source is shown for 15 and 7°N. The values are considered to be less reliable than those at the reference latitude. The residual Z at 15°N (Fig. 3a) is similar to that at 11°N ahead of the trough (categories 2–4). The source ($Z>0$) in the middle troposphere is still present. The large values of the residual at 15°N behind the trough in categories five and six cannot be explained in terms of cumulus eddy transports (cf. Section 4) and are probably artifacts of data inaccuracies. The residual Z at 7°N (Fig. 3b) is quite different from that at 11°N. Ahead of the trough there is a positive residual near the surface and a negative residual in the middle troposphere, in direct opposition to the balance at 11°N. The comparison between Z and the parameterized source term due to cumulus will be made for each latitude in Section 4. Possible causes and magnitudes of the errors due to uncertainties in the analysis will be discussed at that time.

In the above discussion, as in all previous vorticity budget studies, the observed fields of motion were considered to constitute the wave disturbance. Alternatively, the wave disturbances may be considered to be embedded in a basic flow, such as that represented by Burpee and Dugdale (1975, Fig. 2.7) for the mean winds observed during Phase III of GATE. The separation between the wave and the time-averaged basic flow is valid if the time scale over which the mean flow varies, which is on the order of a week, is much longer than the time scale associated with the waves, which is the wave period 3.5 days/$2\pi \approx \frac{1}{2}$ day. However, the requirement for the composite wave is more severe. Since the composite by category designates the phase of the wave either by zonal coordinate or time (where

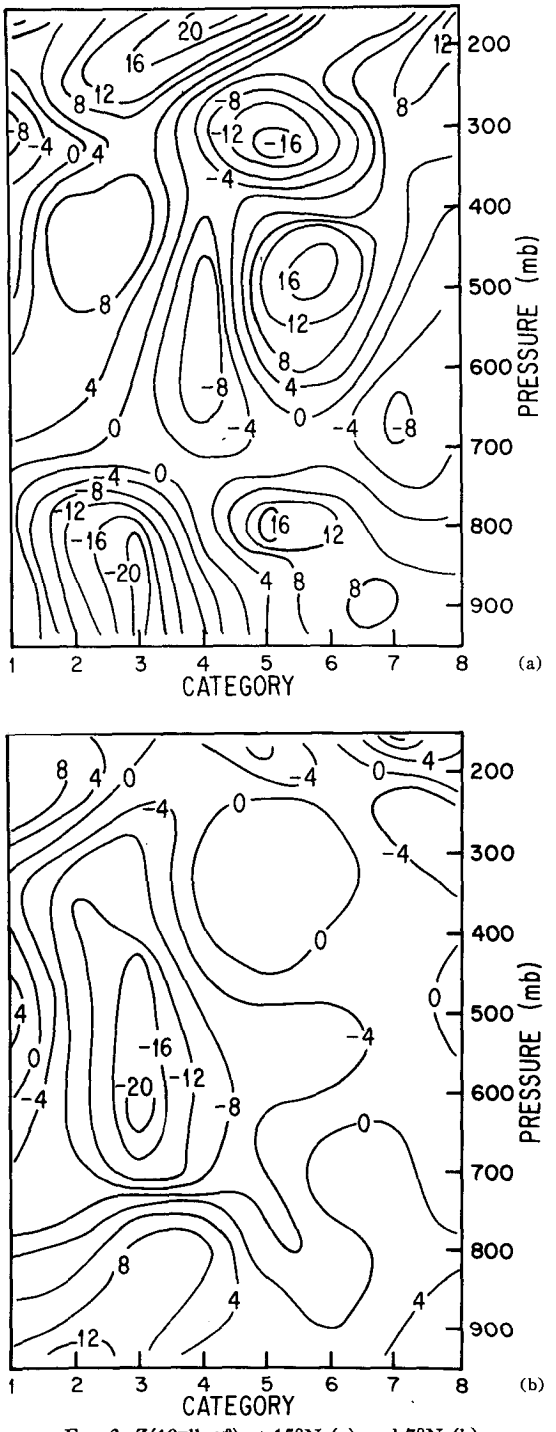

FIG. 3. $Z(10^{-11}$ s$^{-2})$ at 15°N (a) and 7°N (b).

the transformation from one to the other can be made via a constant phase speed, here about -8 m s^{-1}), the zonal average of the composite wave is representative of the (zonally and temporally uniform) basic flow only if the time scale over which the mean flow varies is long *and* the mean flow is approximately zonally uniform. In fact, the interpretation of the composite wave itself can be questioned when the mean flow is zonally nonuniform, since the compositing technique implicitly assumes that the wave and the basic state are nearly uniform zonally and in time. Otherwise the description of an "average" composite wave field that has cyclic zonal and temporal continuity is invalid. Inspection of Burpee and Dugdale's (1975) Phase III average winds indicates that the mean flow is quite zonally uniform at 700 and 500 mb, but is less so at the surface, 850 and 200 mb, where the streamlines and isotachs appear less zonally oriented. The use of the zonally averaged wind below 850 mb or above 250 mb as the basic flow in which the composite wave is embedded appears to be less valid than in the middle troposphere, as does the concept of an average zonally cyclic composite wave.

In order to gain insight into the vorticity budget of the wave disturbance itself, as distinct from the mean flow in which it is embedded, as well as the relation between the wave and the basic state, the wind is decomposed into a zonal mean and deviations from the zonal mean, i.e.,

$$\left.\begin{aligned} \mathbf{V}&=\bar{\mathbf{V}}+\mathbf{V}' \\ \zeta&=\bar{\zeta}+\zeta' \\ \eta&=\bar{\eta}+\eta'=f+\bar{\zeta}+\zeta' \\ \delta&=\nabla\cdot\mathbf{V}=\bar{\delta}+\delta' \\ \omega&=\bar{\omega}+\omega' \end{aligned}\right\}. \tag{3}$$

Zonally averaged quantities are indicated by an overbar and deviations from the zonal mean are denoted by a prime. Consistent with the equivalence of x and t in the compositing technique, the zonal mean fields in (3) are steady.

Substitution of (3) into the large-scale fields in (2) yields

$$\begin{aligned} Z=\zeta'_t+\bar{\mathbf{V}}\cdot\nabla\zeta'+v'\bar{\eta}_y+\mathbf{V}'\cdot\nabla\zeta'+\bar{v}\bar{\eta}_y \\ +\bar{\omega}\zeta'_p+\omega'\bar{\zeta}_p+\omega'\zeta'_p+\bar{\omega}\bar{\zeta}_p+\bar{\eta}\delta'+\zeta'\bar{\delta}+\zeta'\delta'+\bar{\eta}\bar{\delta}, \end{aligned} \tag{4}$$

where large-scale twisting terms have been neglected.

Since the amplitude of v' is 5 m s^{-1}, the nonlinear horizontal advective term $\mathbf{V}'\cdot\nabla\zeta'$ is potentially large. In fact the magnitude of $u'\zeta'_x$ and $v'\zeta'_y$ are both about 10×10^{-11} s^{-2}, nearly half that of ζ'_t. However, Fig. 4 shows that $\mathbf{V}'\cdot\nabla\zeta'$ at 11°N has an amplitude of 3×10^{-11} s^{-2}, about one-third of the terms that individually constitute it. The magnitude of $\mathbf{V}'\cdot\nabla\zeta'$ at 15 and 7°N is also found to be small. The reason for the strong cancellation between the nonlinear advective terms may be found by looking at the streamline patterns for the disturbance wind field $\mathbf{V}'$ shown in RNR's Fig. 4. The amplitude of $\mathbf{V}'$, $u'\zeta'_x$ and $v'\zeta'_y$ are strongest near 850 and 700 mb. The resemblance between the streamline pattern and a single wave component propagating to the west at 850 mb (RNR's Fig. 4b) and to the northwest at 700 mb (RNR's Fig. 4c) is quite striking. Since the waves at these levels are quasi-nondivergent, with $\delta'/\zeta'\leqslant\frac{1}{3}$, the horizontal velocity may be well represented by a streamfunction $\mathbf{V}'=(-\psi_y,\psi_x)$, where $\psi=\psi(kx+ly)$ for a single wave component. The ratio between the zonal and meridional wavenumbers at 700 mb,

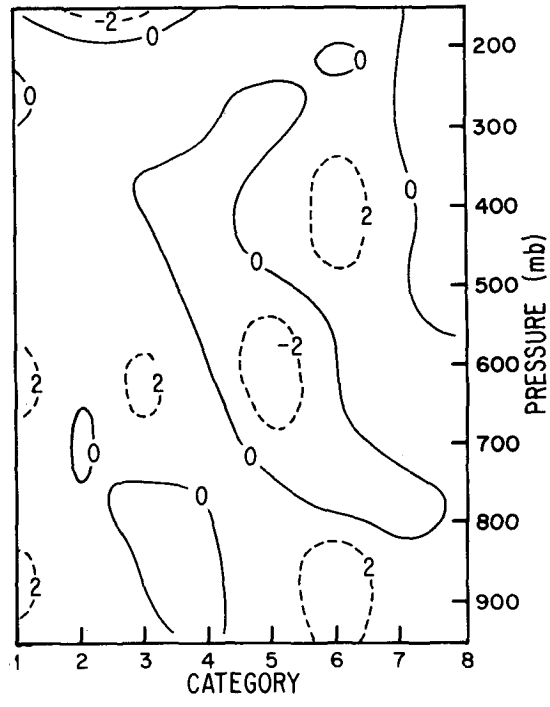

FIG. 4. $\mathbf{V}'\cdot\nabla\zeta'$ at 11°N (10^{-11} s^{-2}).

$$k/l\approx-v'/u'\approx-5\text{ m s}^{-1}/3\text{ m s}^{-1}=-5/3$$

is negative, representing phase lines that slope to the northeast and propagate to the northwest, when time dependence is included. For such a single wave component $\mathbf{V}'\cdot\nabla\zeta'\approx0$, so the approximate cancellation seen between the nonlinear horizontal advective terms is a direct consequence of the existence of a single quasi-nondivergent propagating component. The nonlinear terms $\omega'\zeta'_p$ and $\zeta'\delta'$ are also computed to be small, with magnitudes at most 4×10^{-11} s^{-2}, compared to $\bar{\eta}\delta'$ which has a magnitude of 16×10^{-11} s^{-2}. Thus the wave is well described by linear dynamics, with the nonlinear (wave-wave interaction) terms playing only a small role at this stage of its development.

In order to isolate the dynamics of the wave itself, the quantity $Z-\bar{Z}$ is evaluated. Thus the contributions from the balance that maintains the basic flow are sub-

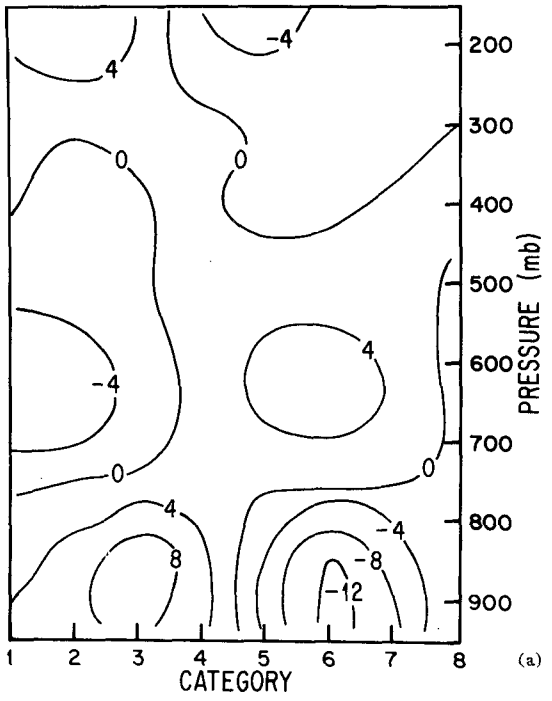

FIG. 5. $\zeta'_t+\bar{\mathbf{V}}\cdot\nabla\zeta'+v'\bar{\eta}_y$ (10^{-11} s^{-2}) at 11°N (a) and 70°N (b).

tracted out:

$$Z-\bar{Z}=\zeta'_t+\bar{\mathbf{V}}\cdot\nabla\zeta'+v'\bar{\eta}_y+(\mathbf{V}'\cdot\nabla\zeta'-\overline{\mathbf{V}'\cdot\nabla\zeta'})$$
$$+\bar{\omega}\zeta'_p+\omega'\bar{\zeta}_p+(\omega'\zeta'_p-\overline{\omega'\zeta'_p})$$
$$+\bar{\eta}\delta'+\zeta'\bar{\delta}+(\zeta'\delta'-\overline{\zeta'\delta'}). \quad (5)$$

Since $\mathbf{V}'\cdot\nabla\zeta'$, $\omega'\zeta'_p$ and $\zeta'\delta'$ are computed to be small, the terms in parentheses are also small. The term $\zeta'\bar{\delta}$ is less than 2×10^{-11} s^{-2} and may be neglected compared to $\bar{\eta}\delta'$. The sum of the linear terms in (5) that do not involve ω or δ and thus are decoupled from the vertical velocity, $\zeta'_t+\bar{\mathbf{V}}\cdot\nabla\zeta'+v'\bar{\eta}_y$, is presented in Fig. 5 for 11 and 7°N. The sum at 15°N is similar to that at 11°N and is not shown. Since the wave is approximately advected at 11°N by the horizontal wind, as illustrated in Fig. 1b and since the nonlinear terms are small, it is not surprising that the sum of the linear terms (Fig. 5a) is less than 7×10^{-11} s^{-2}, except below 800 mb. Since $\zeta'_t\approx24\times10^{-11}$ s^{-2}, the balance is within 30%. However, as indicated in Fig. 6, the wave is apparently not advected at 7°N. The amplitude of $\zeta_t+\mathbf{V}\cdot\nabla\eta$ at 7°N is 15×10^{-11} s^{-2}, which is half that of ζ_t. This is due to the large value of $\bar{v}\bar{\eta}_y$ at that latitude. The mean meridional wind $\bar{v}$ is northerly at 1–2 m s^{-1} at 7°N and the curvature $\bar{\eta}_y$ is large ($\sim4.5\times10^{-11}$ m^{-1} s^{-1}) since it lies on the southern edge of the easterly jet (cf. RNR Fig. 2a). The magnitude of $\bar{v}\bar{\eta}_y$ is about 7×10^{-11} s^{-2} and is much greater than its value at either 11 or 15°N. However, when the contribution from the basic flow is subtracted out it is found that, in fact, the wave is approximately advected by the horizontal wind as a linear disturbance, even at 7°N. As indicated by Fig. 5b the magnitude of $\zeta'_t+\bar{\mathbf{V}}\cdot\nabla\zeta'+v'\bar{\eta}_y$ at 7°N is 8×10^{-11} s^{-2} above 850 mb. This is half the magnitude of $\zeta_t+\mathbf{V}\cdot\nabla\eta$ seen in Fig. 6 and less than 30% of the magnitude of ζ_t. Since $\bar{u}$ in the middle troposphere at 7°N is generally much less than the wave's zonal phase speed of -8 m

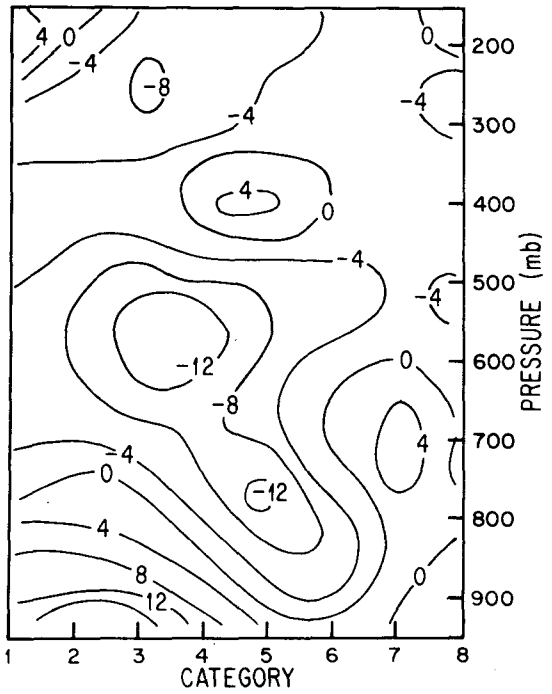

FIG. 6. $\zeta_t+\mathbf{V}\cdot\nabla\eta$ at 7°N (10^{-11} s^{-2}).

s^{-1}, it is clear that the curvature term $v'\bar{\eta}_y$ contributes significantly to the balance at that latitude.

At both 11 and 7°N the divergence term $\bar{\eta}\delta'$ dominates the sum of the linear terms in (5) that are coupled to the vertical velocity, $\bar{\omega}\zeta'_p+\omega'\bar{\zeta}_p+\bar{\eta}\delta'$ (not shown). At 11°N the amplitude of the sum of the "vertical" terms is 18×10^{-11} s^{-2}, about twice the net amplitude of the "horizontal" terms (Fig. 5a), while at 7°N it is 8×10^{-11} s^{-2}, about the same as that of the "horizontal" terms (Fig. 5b).

3. Parameterization of cumulus: Theory

In terms of the subsynoptic-scale eddy quantities, Eq. (2) indicates that

$$Z=-\nabla\cdot(\overline{\mathbf{V}''\zeta''}^{A})-\overline{\omega''\zeta''_p}^{A}-\mathbf{k}\cdot\overline{\nabla\omega''\times\mathbf{V}''_p}^{A}. \quad (6)$$

The first term, which represents the horizontal transport of vorticity by the cumulus-scale eddies, is much smaller than the vertical advective term if the averaging length scale is much greater than the vertical scale. The second and third terms represent the cumulus-scale vertical advection and twisting terms, respectively. When the horizontal eddy transport of vorticity is neglected, Eq. (6) becomes

$$\begin{aligned}Z&=-\overline{\omega''\zeta''_p}^{A}-\mathbf{k}\cdot\overline{\nabla\omega''\times\mathbf{V}''_p}^{A}\\&=-\mathbf{k}\cdot\nabla\times(\overline{\omega''\mathbf{V}''_p}^{A}).\end{aligned} \quad (7)$$

This form is different from that which results when the horizontal eddy transport of momentum is neglected (cf. Schneider and Lindzen, 1976; Stevens *et al.*, 1977). In that case $Z=-\mathbf{k}\cdot\nabla\times(\overline{\omega''\mathbf{V}''})_p^{A}$. The difference between this form and that given in (7) is a term $-\mathbf{k}\cdot\nabla\times\overline{(\omega_p''\mathbf{V}'')}^{A}$, which is not small *a priori*. The form given in (7) must be used in the vorticity budget since gradients of the neglected terms in the momentum equations need not be small.

The correlation between two cloud-scale quantities r'' and s'' may be evaluated approximately as

$$\overline{r''s''}^{A}\approx\sigma(r_c-r)(s_c-s)$$

[cf. Yanai *et al.* (1973), RJ and Anthes' (1977) Eq. (18) with a $(=\sigma)\ll1$], where σ is the fractional area of A covered by clouds, r_c and s_c are the *average* over the area covered by clouds and, as before, $r\equiv\bar{r}^{A}$, $s\equiv\bar{s}^{A}$. A single cloud model has been used, and σ may in general depend on position (x, y and p). The approximation $(rs)_c\approx r_cs_c$ has also been used. As in RJ, ω is assumed to be approximately uniform in the cloud (top-hat profile) so that the cumulus-scale twisting term is neglected. It will be seen below that, in any case, the twisting terms are needed to explain the major part of the large-scale apparent vorticity source, except possibly near the tropopause. Then from Eq. (7),

$$Z\approx-\sigma(\omega_c-\omega)[(\zeta_p)_c-\zeta_p]. \quad (8)$$

In general, if σ were to depend on the vertical coordinate ($\sigma_p\neq0$), an additional identity would be needed to relate $(\zeta_p)_c$, the cloud-averaged vertical gradient of ζ to $(\zeta_c)_p$, the vertical gradient of the cloud-average of ζ. Such an identity is derived in the Appendix [Eq. (A3)]. In the following discussion it will be assumed for simplicity that $\sigma_p=0$ so that $(\zeta_p)_c=(\zeta_c)_p$. In a general formulation the vertical variation of σ could be inferred from a given cumulus mass flux distribution ($M_c=-\sigma\omega_c$) and a cloud model that supplied ω_c. However, the approximation $\sigma_p=0$ is a reasonable one below the tropopause for the present analysis since, as mentioned at the end of this section, predominantly one cloud type—the "deep" clouds that reach from the boundary layer to near the tropopause—is included in the cloud budget.

Using $M_c=-\sigma\omega_c$ and neglecting ω with respect to ω_c, Eq. (8) implies

$$Z\approx M_c(\zeta_c-\zeta)_p. \quad (9)$$

The average vorticity ζ_c in the clouds will be evaluated using a steady-state one-dimensional single cloud model as in RJ. Such a model is the simplest possible that includes stretching of vortex tubes and thus nonconstant ζ_c. Using the notation of RJ, the cloud absolute vorticity η_c is determined from

$$M_c\frac{\partial\eta_c}{\partial p}=\hat{\eta}\frac{\partial M_c}{\partial p} \quad (10)$$

[cf. RJ Eq. (7)], where $\hat{\eta}=\eta_c$ at detraining levels ($M_{cp}>0$) and $\hat{\eta}=\eta$ at entraining levels ($M_{cp}<0$). In-cloud twisting terms have been neglected. In regions of detrainment it has been assumed that average cloud vorticity (η_c) is being detrained. This is only an estimate since cloud properties just inside the cloud boundary could be systematically different from interior properties. However, for a near top-hat profile of cloud vorticity, cloud values of ζ (at any position inside the cloud) approximately equal ζ_c, and ζ_c can be determined from (10) once cloud base values are specified as a boundary condition. The values of vorticity may be locally enhanced at cloud base due to cloud-related convergence and vortex stretching. Rather than apply an *ad hoc* assumption relating cloud-base (p_B) absolute vorticity $\eta_c(p_B)$ to $\eta(p_B)$, the conservative assumption $\eta_c(p_B)=\eta(p_B)$ will be used. The sensitivity of the results presented to $\eta_c(p_B)$ will be discussed in Section 4. With ζ_c determined from (10), the entire parameterized vorticity source term in (9) is determined once M_c is specified. The evaluation of Z given in (9), although an approximation, will give an indication of how well a simple parameterized single-cloud formulation for cumulus-scale eddies accounts for the large-scale residual. Rather than calculate M_c from Z and (10) as was

done by RJ, M_c will be specified from thermodynamic considerations. The comparison of Z with the parameterized form in (9) will be made in Section 4.

The specification of M_c requires further discussion. Profiles of total M_c were provided for all categories and latitudes by R. Johnson. The values were determined from a thermodynamic budget and a spectral cloud model, without downdrafts, using the method described in Johnson (1976). Composite combined region values of temperature, humidity and geopotential were used. Although the inclusion of downdrafts will significantly change the net (updraft plus downdraft) mass flux, especially at lower levels, the mass flux in the updrafts alone will not be significantly affected (R. Johnson, personal communication). Only the vorticity source due to updrafts will be modeled in this study. Standard global radiative cooling profiles (Dopplick, 1972) were used to diagnose M_c. The results presented here were not found to be significantly modified when preliminary values of radiative heating rates determined by R. Johnson from composite cloud cover and data from Albrecht and Cox (1975) were used. Not all cloud types in the spectral representation are expected to contribute to the vorticity balance. The shallow, narrow cumuli, which detrain at low levels, may rapidly adjust to the environment and not contribute significantly to the large-scale vorticity balance (Schneider and Lindzen, 1976). In fact RJ, diagnosing M_c from a vorticity budget and a single-cloud model, found profiles of M_c that suggested only deep convection contributed to the vorticity budget. Contributions from updrafts and downdrafts may have effectively cancelled at low levels, leading to their result. Since only updrafts are modeled in this (and RJ's) study, shallow clouds must be excluded. The spectral cloud model used in determining M_c and the single-cloud model used in (9) and (10) are not formally consistent. However, since only clouds detraining above a certain level are expected to contribute to the vorticity balance, these "deep" clouds may be considered a single-cloud type and may be reasonably represented by a single M_c as in (10).

4. Parameterization of cumulus: Comparison between apparent vorticity source and parameterized form

In this section a comparison will be made between the values of Z computed from the large-scale residual, as described in Section 2, and the parameterized vorticity source due to cumulus specified in Eq. (9). Possible sources of error in Z due to the data analysis include nonstationarity and zonal nonuniformity of the individual waves, both leading to distortion in the composite fields. As discussed in Section 2, these errors are expected to be most pronounced below 850 mb and above 250 mb. Errors due to kinematically adjusted ω's will be largest near the tropopause. The phases of the waves were computed relative to 700 mb at the reference latitude, near 11°N. Although the waves were allowed to determine their own tilt (RNR Section 2), any differential phase propagation from one altitude or latitude to the next would produce distortion in the composite waves. Interference from propagating systems with time and spatial scales similar to those of the composited wave will also produce errors.

Although it is difficult to put numerical values on the errors inherent in the compositing technique, an *a posteriori* estimate can be made of the error due to zonal nonuniformity. It is obvious from the preceding discussion that the errors should be minimized near the disturbance vorticity center, at about 11°N and 700 mb. RNR's Table 2 indicates that when the waves were composited separately over land and ocean, the average 850 mb vorticities near the disturbance center differed by 4.2×10^{-6} s^{-1}. This gradient in vorticity occurred over a distance of about 1000 km, which translates into a value of $\zeta_t=$ (phase speed)$\times\zeta_x\approx 8$ m s$^{-1}\times 4.2\times10^{-6}$ s$^{-1}/10^6$ m$\approx 3.4\times10^{-11}$ s^{-1}. Thus, zonal variations in the magnitude of the vorticity, which will not be present in the combined region composite, will lead to errors in Z on the order of 3.4×10^{-11} s^{-1}, which is about 35% of the maximum value of ζ_t at that level ($\sim 10\times10^{-11}$ s^{-1}). Although this is only a crude estimate of one source of error inherent in the analysis, it should be reliable at least as a lower bound. Errors at latitudes other than the reference latitude are probably much greater. Thus, care must be taken in making more than a qualitative comparison between Z and the parameterized vorticity source, especially away from 11°N.

The total mass flux for clouds detraining at all levels had a maximum near the surface. Since only deep clouds may contribute to the large-scale vorticity budget, total M_c profiles were provided by R. Johnson for all clouds that detrained above a certain level. M_c profiles were computed for clouds detraining above 850, 750 and 500 mb for comparison. Using (10), values of $M_c(\zeta_c-\zeta)_p$ were computed and comparison was made with Z at 11°N. The values of $M_c(\zeta_c-\zeta)_p$ for the three M_c profiles were quite similar above 600 mb. However, the large maximum in Z seen in Fig. 2 near 650 mb was completely absent when only clouds detraining above 500 mb were included and was best resolved when clouds detraining above 750 mb were included. In fact, inspection of profiles of cloud-base mass flux as a function of detrainment level in Fig. 5 of Johnson (1978) indicates that the bimodal cloud distribution has a sharp upper-level maximum at 200 mb, and a low-level maximum that becomes negligible (below one-tenth of its maximum value) above approximately 750 mb so that this is the cutoff level for "shallow" clouds. In the following only profiles of total M_c will be considered for all clouds detraining above 750 mb (Fig. 7).

The profile of ζ_c at 11°N, computed from (10), $\eta_c(p_B)=\eta(p_B)$, a cloud base level of 950 mb and the

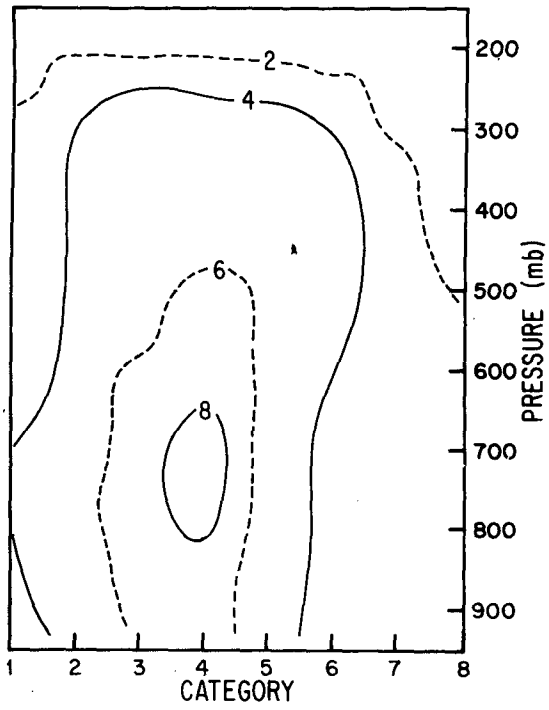

FIG. 7. Cumulus mass flux M_c (mb h^{-1}) at 11°N for all clouds detraining above 750 mb.

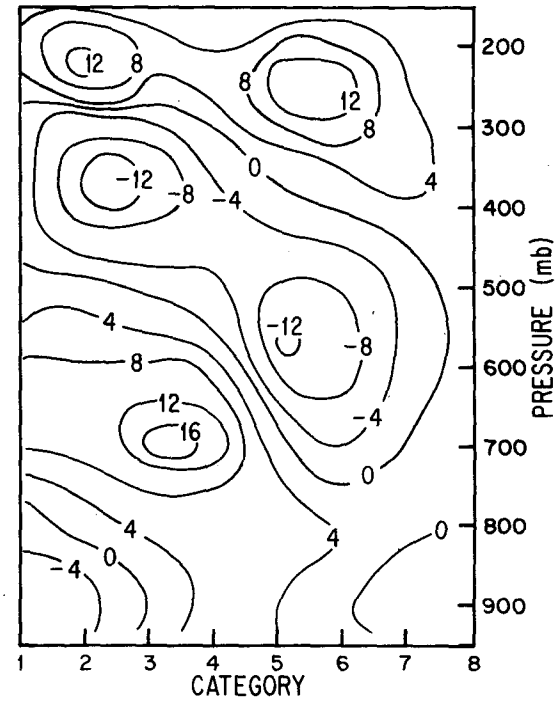

FIG. 9. $M_c(\zeta_c-\zeta)_p$ at 11°N (10^{-11} s^{-2}).

M_c's shown in Fig. 7 is presented in Fig. 8. Here ζ_c is of the same order as ζ (cf. RNR's Fig. 8c). The negative values of ζ_c in the upper troposphere result directly from (10), where η_c approaches zero as M_c goes to zero in the detrainment region near the tropopause (150 mb). When $\eta_c=0$, $\zeta_c=-f=-2.8\times10^{-5}$ s^{-1} at 11°N.

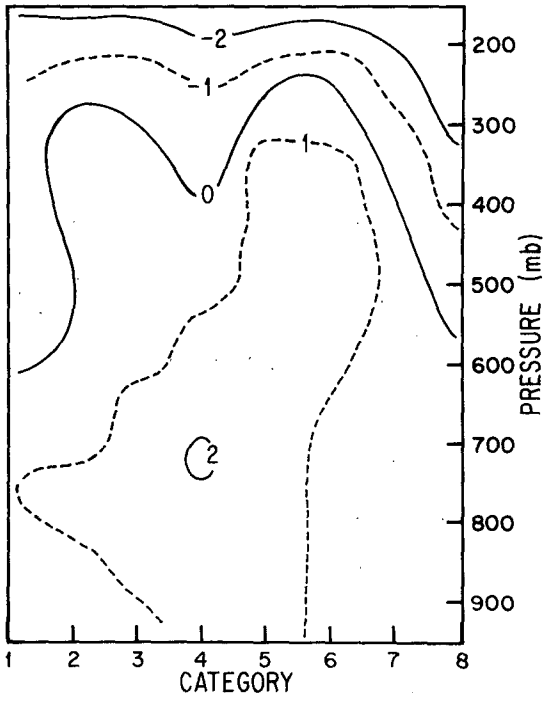

FIG. 8. Cloud vorticity ζ_c at 11°N (10^{-11} s^{-2}).

The parameterized vertical advection term due to cumulus-scale processes is shown in Fig. 9 for 11°N. The maxima and minima in Z (Fig. 2) near category 3 near 200, 400 and 650 mb are all reflected in $M_c(\zeta_c-\zeta)_p$, with a smaller magnitude. At 200 mb the maximum in Z is underestimated by a factor of 2. The only other major discrepancy is the complete absence of the negative values seen in Z near the surface near category 5. The reduced reliability of the composite wave outside the middle troposphere was discussed in Section 2. Since the first data level above the surface in this data set is at 850 mb, it is most likely that the negative values near the surface are a reflection of boundary layer dissipative processes that are interpolated into the cloud layer. If more data levels were included in the lower troposphere, the negative values of Z near 900 mb would be significantly reduced. It is considered that the values of Z near 200 mb may be substantially in error since the wave was composited with respect to the 700 mb level. Vertical variations of σ may also be important near the tropopause, where clouds lose their buoyancy. However, cumulus-scale twisting effects (neglected in this study) may also contribute to the large-scale residual at this level. The effect of variation in the assumed value of $\eta_c(p_B)$ will be discussed later. The cumulus term $M_c(\zeta_c-\zeta)_p$ for latitudes 15 and 7°N is shown in Figs. 10a and 10b for comparison with Figs. 3a and 3b. The positive values of Z near the surface evident at both 7 and 15°N could not be accounted

for by boundary layer dissipative processes and thus indicate the large magnitude of the errors in Z away from the reference latitude. At 15°N, the minima in the residual Z (Fig. 3a) seen near the ground near category 3 and in the middle troposphere near category 5, and the maxima near category 3 near 500 and 200 mb are all reflected, qualitatively, in the parameterized term (Fig. 10a). However, the large positive values of Z that dominate the region behind the trough (categories 5–6) have no counterpart in the parameterized term. There is no significant cumulus mass flux at this phase of the wave. Thus it is believed that these positive values are due to data inaccuracies rather than any physical process. At 7°N, the extrema in Z (Fig. 3b) seen near category 3 near the ground (positive), 600 mb (negative) and 200 mb (positive) are all reflected, at least qualitatively, in the parameterized term (Fig. 10b). Once again, data at this latitude are less reliable than at 11°N.

The agreement between Z and $M_c(\zeta_c-\zeta)_p$ at 11°N is within 30% in the middle troposphere, and is probably within data uncertainties, as discussed at the beginning of this section. Thus cumulus-scale twisting effects are not needed to explain the large-scale apparent vorticity source, except perhaps near the tropopause, where $M_c(\zeta_c-\zeta)_p$ underestimates Z by a factor of 2. However the disagreement between Z and $M_c(\zeta_c-\zeta)_p$ near the tropopause may also be due to data inaccuracies (which may be very large at that level), vertical variations of σ (which may also be large at that level), or errors in $\eta_c(p_B)$ (discussed below) as well as errors in M_c. It can be concluded that if only deep clouds are used to prescribe M_c, the simple cloud model in (10) with $\eta_c(p_B)=\eta(p_B)$ and the simple parameterized term $M_c(\zeta_c-\zeta)_p$ well represent the apparent vorticity source Z for the composite wave at 11°N throughout most of the troposphere.

The comparison between $M_c(\zeta_c-\zeta)_p$ and Z at 11°N presented here was found to improve in certain respects when cloud base absolute vorticities $\eta_c(p_B)$ twice as large were assumed (not shown). With $\eta_c(p_B)=2\eta(p_B)$ the parameterized apparent vorticity source near 200 mb increased to a maximum of 24×10^{-11} s^{-2}, more closely agreeing with Z near the trough (but not near the ridge), while the maximum near 650 mb increased to 22×10^{-11} s^{-2}, also more closely agreeing with Z. With $\eta_c(p_B)=2\eta(p_B)$, cloud-base *relative* vorticities $\zeta_c(p_B)$ correspondingly increased to a maximum of 5×10^{-5} s^{-1}, a factor of more than 3 greater than the value of $\zeta(p_B)$. An increase of $\eta_c(p_B)$ by a factor of 4 was found to produce values of $M_c(\zeta_c-\zeta)_p$ very much larger than Z at all levels. Thus values of the parameterized apparent vorticity source are somewhat sensitive to moderate increases in $\eta_c(p_B)$, especially near the tropopause, while an overestimation of $\eta_c(p_B)$ significantly overestimates the vorticity source at all levels. Good agreement was found between $M_c(\zeta_c-\zeta)_p$ and Z in the middle troposphere when $\eta_c(p_B)=\eta(p_B)$ was assumed.

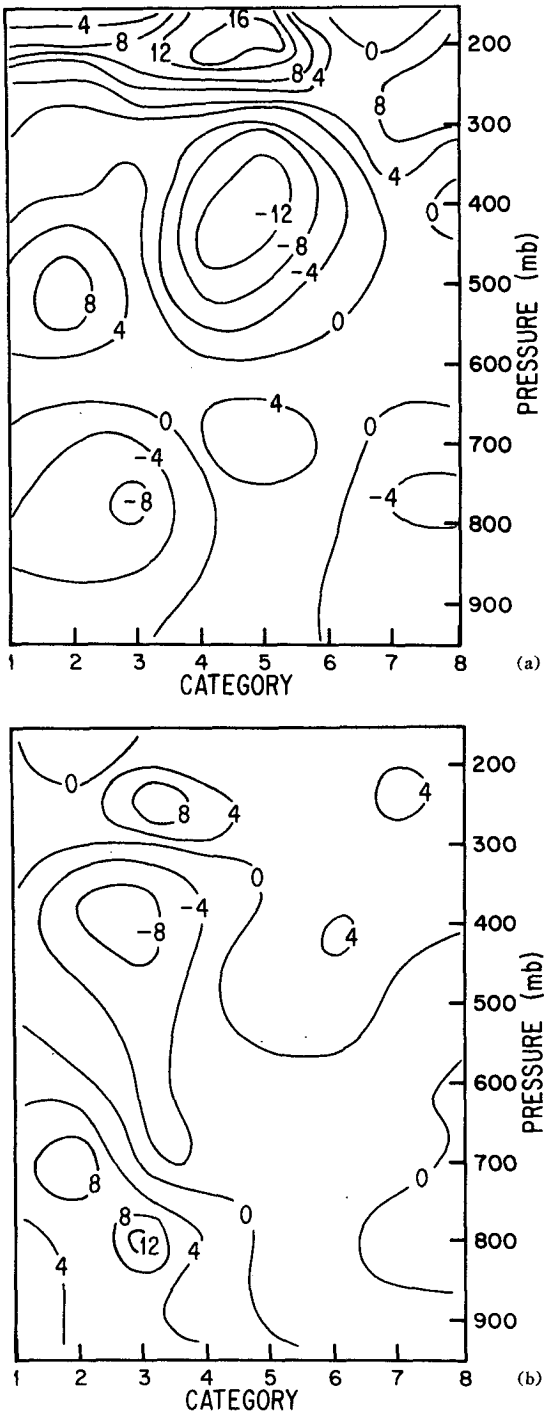

FIG. 10. $M_c(\zeta_c-\zeta)_p$ (10^{-11} s^{-2}) at 15°N (a) and 7°N (b).

Such a conservative assumption appears to be the best approximation available, especially given the lack of a general method for diagnosing $\eta_c(p_B)$. The extent to which the discrepancy near the tropopause is data related and not physical cannot be resolved in this study.

It should be noted that the comparison between the

parameterized form of the vorticity source and Z presented here may be quite different than that which results when ζ_c is assumed constant with height (Stevens *et al.*, 1977). In that case, since there is no production of cloud vorticity by vortex stretching, the effect of cumulus may be underestimated. In particular, the parameterized form used in Stevens *et al.* (1977), neglecting twisting-like terms, is $-M_c\zeta_p+\partial M_c/\partial p(\zeta_{cc}-\zeta)$, where ζ_{cc} is the constant vorticity. This may be very different from $M_c(\zeta_c-\zeta)_p$ if $\hat{\eta}=f+\hat{\zeta}\neq\zeta_{cc}-\zeta$ [cf. (10)]. Note that $\zeta_{cc}-\zeta$ omits any effect of planetary vorticity. At 11°N the differences between the parameterized form used in the present study and that used by Stevens *et al.* (1977) are significant. The latter (not shown) poorly represents the apparent vorticity source near 650 mb, a significant feature for the vorticity budget.

5. Conclusion

In this study we have found that the vorticity balance of the composite African wave is linear, with the nonlinear horizontal advective terms approximately cancelling due to the presence of a quasi-nondivergent single-propagating wave component. Thus nonlinearities are apparently not important for the dynamics of the "average" Atlantic easterly wave at this early stage of its development. We have also found that the linear waves are approximately advected by the horizontal wind at all levels above 850 mb, even to the south of the easterly jet where the mean zonal wind is small. This agrees with the hypothesized dynamic organization of the pre-storm stage easterly wave given in Shapiro (1977). The curvature term $v'\bar{\eta}_y$ contributes significantly to the balance. The vorticity divergence term dominates the terms that couple to the vertical velocity. The reason for the approximate balance among terms that are decoupled from the vertical velocity, despite the presence of large vorticity divergence and cumulus transports, has not been resolved.

In this study we have also found that the parameterized form $M_c(\zeta_c-\zeta)_p$ for the vorticity source due to cumulus, when coupled with a single-cloud model with $\eta_c(p_B)=\eta(p_B)$, and when M_c is specified from a thermodynamic budget for only deep clouds, accounts well for most features of the apparent vorticity source Z obtained from the large-scale budget. The large apparent source ahead of the trough at 11°N in the middle troposphere is reflected in the parameterized form. The major discrepancies at 11°N are the absence of a vorticity sink near the surface (probably due to boundary layer friction) in the parameterized form and the underestimation of the apparent source near the tropopause. The cumulus-scale twisting effect does not contribute significantly to the vorticity balance, except perhaps near 200 mb. The interpretation of the apparent vorticity source given in RJ as simply a removal of vorticity-rich low-level air by the cumulus to upper levels must be modified for the African wave, due to the strong mid-tropospheric vorticity source found in this study. However, the successful modeling of all the qualitative features of Z, including the mid-tropospheric source, by an extremely simple single-cloud model is encouraging. A cloud model for ζ_c is vital, since without the production of cloud vorticity by vortex tube stretching, the vorticity source may be significantly underestimated. The use of a more complex cloud model, including spectral (or bulk) updrafts and downdrafts, does not seem warranted considering the inaccuracies inherent in the present data set. If a more accurate data set were used, such as that derived from GATE A/B-scale data, a study analogous with the present one could help resolve features of the vorticity structure in downdrafts as well as vorticity values at cloud base.

A remaining theoretical question is the relation between the parameterization of cumulus transports in the momentum equations and the vorticity or divergence equation. The resolution of the difference between the results when the horizontal eddy flux of momentum or vorticity is neglected [cf. discussion following Eq. (7)] has not been completely made. The relation between the cloud budget vorticity [e.g., Eq. (9)] and a cloud budget of momentum must also be clarified.

Acknowledgment. The author kindly thanks Prof. Richard Reed, Mr. Donald Norquist and Mr. Ernest Recker for providing the composite wave data, and Dr. Richard Johnson for providing the cumulus mass fluxes, used in this study. Dr. Duane Stevens made some valuable comments on an earlier version of this paper.

APPENDIX

Derivation of Leibnitz-Like Law

Using the definition of the "running" area average, i.e.,

$$(\overline{\ })^A \equiv \frac{1}{A}\int_{x-\Delta x/2}^{x+\Delta x/2}\int_{y-\Delta y/2}^{y+\Delta y/2}(\ )dx'dy',$$

where $A=\Delta x\Delta y$, $\overline{(r_p)}^A=(\bar{r}^A)_p$ follows trivially for any quantity r. Then since

$$(\overline{r''^2}^A)_p\approx[\sigma(r_c-r)^2]_p$$
$$=(r_c-r)^2\sigma_p+2\sigma(r_c-r)[(r_c)_p-r_p] \quad \text{(A1)}$$

and

$$(\overline{r_p''^2})^A=2\overline{r''r_p''}^A\approx 2\sigma(r_c-r)[(r_p)_c-r_p] \quad \text{(A2)}$$

are equal,

$$(r_p)_c\approx(r_c)_p+[(r_c-r)\sigma_p]/2\sigma. \quad \text{(A3)}$$

This Leibnitz-like law relates the average vertical gradient of any quantity in the cloud $(r_p)_c$ to the

vertical gradient of the average in the cloud $(r_c)_p$ and the vertical gradient of the area covered by cloud σ_p. The approximations $(r^2)_c \approx (r_c)^2$ and $(rr_p)_c \approx r_c(r_p)_c$ have been used. These will be satisfied if r in the cloud has nearly a top-hat profile. An analogous assumption is made for the cloud environment. With $r=\zeta$, (A3) could be used in Eq. (8) to relate $(\zeta_p)_c$ to $(\zeta_c)_p$.

Eq. (A3) may be alternatively derived by direct application of Leibnitz's rule, $(r_p)_c = (r_c)_p + [(r_c - r_B)\sigma_p]/\sigma$. Here r_B, the value of r on the cloud boundary, is taken to be the average of r inside the cloud (r_c) and in the environment $(\sim \bar{r}^A)$. That is, $r_B \approx (r_c + \bar{r}^A)/2$ so that (A3) follows.

REFERENCES

Albrecht, B., and S. Cox, 1975: The large-scale response of the tropical atmosphere to cloud-modulated infrared heating. *J. Atmos. Sci.*, **32**, 16–24.

Anthes, R., 1977: A cumulus parameterization scheme utilizing a one-dimensional cloud model. *Mon. Wea. Rev.*, **105**, 270–286.

Burpee, R., 1975: Some features of synoptic-scale waves based on compositing analysis of GATE data. *Mon. Wea. Rev.*, **103**, 921–925.

——, and G. Dugdale, 1975: A summary of weather systems affecting western Africa and the eastern Atlantic during GATE. Report on the Field Phase of the GARP Atlantic Tropical Experiment Scientific Program, GATE Rep. No. 16, 2.1–2.42.

Dopplick, T., 1972: Radiative heating of the global atmosphere. *J. Atmos. Sci.*, **29**, 1278–1294.

Hawkins, H., 1972: Development of a seven-level balanced, diagnostic model and its application to three disparate tropical disturbances. NOAA Tech. Memo. ERL NHRL-98, 207 pp. [NTIS COM-72-10330.]

Johnson, R., 1976: The role of convective-scale precipitation downdrafts in cumulus and synoptic-scale interactions. *J. Atmos. Sci.*, **33**, 1890–1910.

——, 1978: Cumulus transports and their meridionally varying response to large-scale forcing in an African tropical wave disturbance composite for Phase III of GATE. *J. Atmos. Sci.*, **35**, 484–494.

Norquist, E., E. Recker and R. Reed, 1977: The energetics of African wave disturbances as observed during Phase III of GATE. *Mon. Wea. Rev.*, **105**, 334–342.

Reed, R., and E. Recker, 1971: Structure and properties of synoptic-scale wave disturbances in the equatorial western Pacific. *J. Atmos. Sci.*, **28**, 1117–1133.

——, and R. Johnson, 1974: The vorticity budget of synoptic-scale wave disturbances in the tropical western Pacific. *J. Atmos. Sci.*, **31**, 1784–1790.

——, D. Norquist and E. Recker, 1977: The structure and properties of African wave disturbances as observed during Phase III of GATE. *Mon. Wea. Rev.*, **105**, 317–333.

Ruprecht, E., and W. Gray, 1976: Analysis of satellite-observed tropical clusters. I. Wind and dynamic fields. *Tellus*, **28**, 391–413.

Schneider, E., and R. Lindzen, 1976: A discussion of the parameterization of momentum exchange by cumulus convection. *J. Geophys. Res.*, **81**, 3158–3160.

Shapiro, L., 1977: Tropical storm formation from easterly waves: A criterion for development. *J. Atmos. Sci.*, **34**, 1007–1021.

Stevens, D., R. Lindzen and L. Shapiro, 1977: A new model of tropical waves incorporating momentum mixing by cumulus convection. *Dyn. Atmos. Oceans*, **1**, 365–425.

Yanai, M., and T. Nitta, 1967: Computation of vertical motion and vorticity budget in a Caribbean easterly wave. *J. Meteor. Soc. Japan*, **45**, 444–466.

——, M., S. Esbensen and J.-H. Chu, 1973: Determination of bulk properties of tropical cloud clusters from large-scale heat and moisture budgets. *J. Atmos. Sci.*, **30**, 611–627.